

Adaptive Finite Element Simulation of the Time-dependent Simplified P_N Equations

Martin Frank* Jens Lang[†] Matthias Schäfer[‡]

January 20, 2009

Abstract

The steady-state simplified P_N approximation to the radiative transport equation has been successfully applied to many problems involving radiation. Recently, time-dependent simplified P_N equations have been derived by an asymptotic analysis similar to the asymptotic derivation of the steady-state SP_N equations [7]. In this paper, we present computational results for the time-dependent SP_N equations in two dimensions, obtained by using an adaptive finite element approach. Several numerical comparisons with other existing models are shown.

1 Introduction

Time-dependent radiative transfer, described by the radiative transfer equation, is hard to compute. This is due to the six-dimensional phase space ($1 \times$ time, $2 \times$ angle, $3 \times$ space). There is an interest in time-dependent radiative transfer solutions, e.g. in astrophysics (supernova explosions), the interaction of short-pulsed lasers with plasmas, and light detection and ranging (LIDAR). It is our purpose in this paper to numerically investigate the time-dependent simplified P_N equations in two dimensions. These models have been very successful in the steady case. Here we investigate an extension to the time-dependent case.

*TU Kaiserslautern, Fachbereich Mathematik, Erwin-Schrödinger-Str., 67663 Kaiserslautern, Germany, frank@mathematik.uni-kl.de

[†]TU Darmstadt, Fachbereich Mathematik, Schlossgartenstrasse 7, 64289 Darmstadt, Germany, lang@mathematik.tu-darmstadt.de

[‡]Fraunhofer ITWM, Fraunhoferplatz 1, 67663 Kaiserslautern, Germany, matthias.schaefer@itwm.fhg.de

The simplified P_N (SP_N) equations were originally developed for steady-state problems in nuclear engineering [8, 9, 10] and have subsequently been generalized and successfully applied in several other fields, including radiative transfer [13, 18, 19]. The first formal derivation by Gelbard [8, 9, 10] started with the one-dimensional P_N equations, which contain only first-order space derivatives, and used substitutions to obtain a system of elliptic partial differential equations. To obtain equations in three space dimensions, even-order moments are interpreted as scalars, odd-order moments are interpreted as vectors, and one-dimensional derivatives ∂_x are replaced by divergence operators and gradients respectively. In three space dimensions, compared to the $(N + 1)^2$ independent unknowns in the spherical harmonics P_N equations, the number of unknowns in the SP_N equations increases only linearly with N . Because of the derivation via the one-dimensional P_N equations, the SP_N method was at first not widely accepted. But alternative derivations via asymptotic expansion [17] and via a variational approach [2, 23] have substantiated the validity of the SP_N hierarchy.

The SP_N equations are accurate if the medium is optically thick, the scattering rate is comparable to the collision rate, and scattering is not highly forward-peaked [17]. In addition, numerical experiments (cf. [19] and references therein) have shown that the SP_N equations give good results even when the regime is not so diffusive, and even in the presence of a discontinuity in the opacities. This means that in the diffusive regime a higher accuracy is obtained and at the same time the range of applicability is increased.

Until recently, the SP_N method was almost exclusively applied to steady-state transport equations, i.e. no time dependence was assumed. Only then can the P_N equations be substituted into each other to give a second-order system. To our knowledge, there has been only one attempt in the literature [21] to apply the SP_N method to a time-dependent problem. Here, the authors use a semi-discretization in time (i.e. the time variable is discretized whereas the other variables are treated as being continuous) and apply the SP_N approximation to the then steady system. This paper, on the other hand, investigates time-dependent SP_N equations which were systematically derived from the Boltzmann equation using an asymptotic analysis.

The numerical solution of the SP_N equations are often still quite expensive due to their inherent multi-scale structure in both time and space. A remedy is to use fully adaptive algorithms where the local accuracy of the numerical solution is controlled by means of a posteriori error estimates in space and time. Such estimators are well established to control the adaptive multilevel process producing highly refined space-time grids to capture local effects efficiently and therefore drastically reducing the size of the arising linear algebraic systems with respect to a prescribed tolerance. We apply the adaptive Rothe method based on the discretization sequence first in time then in space, in contrast to the usual Method of Lines approach (see e.g. [14] and references therein). The spatial discretization is considered as a perturbation of the time integration process. Implementations have been done in the KARDOS library [6], which provides a suitable programming environment for adaptive algorithms to solve nonlinear time-dependent PDEs.

This paper is organized as follows: A brief summary of the derivation of the time-dependent SP_N equations using asymptotic analysis is given in Section 2. Suitable initial and boundary conditions are stated in Section 3. The employed numerical method is described in Section 4. In Section 5, these techniques are applied to two test cases from the recent radiative transfer literature.

2 Time-Dependent SP_N Equations

We consider a convex, open, bounded domain Z in \mathbb{R}^3 , and we assume that Z has a smooth boundary with outward normal vector n . The direction of particle motion is given by $\Omega \in S^2$, where S^2 is the unit sphere in three dimensions. Moreover, we let

$$\Gamma = \partial Z \times S^2 \quad \text{and} \quad \Gamma^- = \{(x, \Omega) \in \Gamma : n(x) \cdot \Omega < 0\}.$$

The transport of mono-energetic particles that undergo isotropic scattering in a medium is modeled by the linear Boltzmann equation

$$\frac{1}{v} \partial_t \psi(t, x, \Omega) + \Omega \cdot \nabla_x \psi(t, x, \Omega) + \sigma_t(x) \psi(t, x, \Omega) = \frac{\sigma_s(x)}{4\pi} \int_{S^2} \psi(t, x, \Omega') d\Omega' + \frac{q(t, x)}{4\pi}, \quad (2.1)$$

where q is an isotropic source term. At the boundary, we prescribe the ingoing radiation

$$\psi(t, x, \Omega) = \psi_b(t, x, \Omega) \quad \text{on} \quad \Gamma^-, \quad (2.2)$$

and as the initial condition, we prescribe

$$\psi(0, x, \Omega) = \psi_0(x, \Omega). \quad (2.3)$$

Here, $\psi(t, x, \Omega) \cos \theta dA dt d\Omega$ is the number of particles at point x and time t that move with velocity v during dt through an area dA into a solid angle $d\Omega$ around Ω , and θ is the angle between Ω and dA . The total cross section $\sigma_t(x)$ is the sum of the absorption cross section $\sigma_a(x)$ and the total scattering cross section $\sigma_s(x)$.

The time-dependent SP_N equations have been derived in [7]. For the convenience of the reader, we here present an abbreviated version which contains the major ideas. The steady-state diffusion equation is an elliptic PDE. Time-dependent diffusion theory is governed by a parabolic PDE. To obtain higher-order corrections to diffusion theory, we write the transport equation in a parabolic scaling. Space-derivatives are scaled by a small parameter ε and the additional time-derivative is scaled by ε^2 . This is called a parabolic scaling, since a differential operator that is first-order in time and second-order in space is invariant under this scaling. The transport equation is therefore written as:

$$\varepsilon^2 \frac{1}{v} \partial_t \psi + \varepsilon \Omega \cdot \nabla_x \psi + \sigma_t \psi = (\sigma_t - \varepsilon^2 \sigma_a) \frac{1}{4\pi} \phi + \varepsilon^2 \frac{q}{4\pi}, \quad (2.4)$$

where $\psi = \psi(t, x, \Omega)$, $\phi(t, x) = \int_{S^2} \psi(t, x, \Omega) d\Omega$, and $q = q(t, x)$.

Integrating (2.4) over Ω and dividing by ε^2 , we obtain the “balance” equation

$$\frac{1}{v} \partial_t \phi + \frac{1}{\varepsilon} \nabla_x \cdot \int_{S^2} \Omega \psi d\Omega + \sigma_a \phi = q, \quad (2.5)$$

which states a basic physical principle: changes in the scalar flux ϕ are either due to leakage (the spatial derivative term), absorption, or sources. We require that this “balance” equation be contained in the final choice of SP_N equations.

We write (2.4) as

$$(1 + \varepsilon \Omega \cdot X + \varepsilon^2 T) \psi = S, \quad (2.6)$$

where

$$X = \frac{1}{\sigma_t} \nabla_x, \quad T = \frac{1}{v \sigma_t} \partial_t, \quad \text{and} \quad S = \left(1 - \varepsilon^2 \frac{\sigma_a}{\sigma_t}\right) \frac{\phi}{4\pi} + \varepsilon^2 \frac{q}{4\pi \sigma_t}. \quad (2.7)$$

We start by expanding the inverse of the operator in (2.6) in powers of ε

$$\begin{aligned} \psi &= (1 + \varepsilon \Omega \cdot X + \varepsilon^2 T)^{-1} S \\ &= \{1 - (\Omega \cdot X) \varepsilon + [-T + (\Omega \cdot X)^2] \varepsilon^2 + [(\Omega \cdot X)T + (T - (\Omega \cdot X)^2)(\Omega \cdot X)] \varepsilon^3 \\ &\quad + [(T - (\Omega \cdot X)^2)T + (-2(\Omega \cdot X)T + (\Omega \cdot X)^3)(\Omega \cdot X)] \varepsilon^4 \dots\} S + \mathcal{O}(\varepsilon^5). \end{aligned} \quad (2.8)$$

In the following we assume that the system is homogeneous, i.e. σ_a and σ_t are constant. This assumption is crucial for the validity of the following analysis. For a discussion of the non-homogeneous case, we refer the reader to the end of this section. Integrating (2.8) with respect to Ω and using

$$\int_{S^2} (\Omega \cdot X)^n d\Omega = [1 + (-1)^n] \frac{2\pi}{n+1} X^n = [1 + (-1)^n] \frac{2\pi}{n+1} (X \cdot X)^{\frac{n}{2}}, \quad (2.9)$$

we obtain

$$\begin{aligned} \phi &= \int_{S^2} \psi d\Omega \\ &= 4\pi \left\{ 1 + \left(\frac{1}{3} X^2 - T\right) \varepsilon^2 + \left(T^2 + \frac{1}{5} X^4 - TX^2\right) \varepsilon^4 \right. \\ &\quad \left. + \left(\frac{1}{7} X^6 + 2T^2 X^2 - T^3 - TX^4\right) \varepsilon^6 \right\} S + \mathcal{O}(\varepsilon^8). \end{aligned} \quad (2.10)$$

Hence,

$$\begin{aligned}
4\pi S &= \left\{ 1 + \left(\frac{1}{3}X^2 - T \right) \varepsilon^2 + \left(T^2 + \frac{1}{5}X^4 - TX^2 \right) \varepsilon^4 \right. \\
&\quad \left. + \left(\frac{1}{7}X^6 + 2T^2X^2 - T^3 - TX^4 \right) \varepsilon^6 \right\}^{-1} \phi + \mathcal{O}(\varepsilon^8) \\
&= \left\{ 1 + \left(-\frac{1}{3}X^2 + T \right) \varepsilon^2 + \left(-\frac{4}{45}X^4 + \frac{1}{3}TX^2 \right) \varepsilon^4 \right. \\
&\quad \left. + \left(-\frac{44}{945}X^6 - \frac{1}{3}T^2X^2 + \frac{4}{15}TX^4 \right) \varepsilon^6 \right\} \phi + \mathcal{O}(\varepsilon^8). \tag{2.11}
\end{aligned}$$

Inserting the definition of the source term S from (2.7), we get

$$\begin{aligned}
\left(1 - \varepsilon^2 \frac{\sigma_a}{\sigma_t} \right) \phi + \varepsilon^2 \frac{q}{\sigma_t} &= \left\{ 1 + \left(-\frac{1}{3}X^2 + T \right) \varepsilon^2 + \left(-\frac{4}{45}X^4 + \frac{1}{3}TX^2 \right) \varepsilon^4 \right. \\
&\quad \left. + \left(-\frac{44}{945}X^6 - \frac{1}{3}T^2X^2 + \frac{4}{15}TX^4 \right) \varepsilon^6 \right\} \phi + \mathcal{O}(\varepsilon^8). \tag{2.12}
\end{aligned}$$

Deleting ϕ on both sides and multiplying by σ_t/ε^2 , we obtain

$$\begin{aligned}
-\sigma_a \phi + q &= \sigma_t T \phi - \frac{\sigma_t}{3} X^2 \left[\phi - \varepsilon^2 T \phi + \frac{4}{15} \varepsilon^2 X^2 \phi \right. \\
&\quad \left. + \frac{44}{315} \varepsilon^4 X^4 \phi + \varepsilon^4 T^2 \phi - \frac{4}{5} \varepsilon^4 T X^2 \phi \right] + \mathcal{O}(\varepsilon^6). \tag{2.13}
\end{aligned}$$

We note that this equation has the form of the balance equation (2.5). Since we want to keep this form, in the subsequent approximations we only manipulate the terms within the brackets.

2.1 SP_1 Approximation

For the lowest-order approximation, we neglect terms of order $\mathcal{O}(\varepsilon^2)$. Then (2.13) becomes the classical diffusion (SP_1) equation

$$\frac{1}{v} \partial_t \phi = \frac{1}{3\sigma_t} \nabla_x^2 \phi - \sigma_a \phi + q. \tag{2.14}$$

2.2 SP_3 Approximation

As in the steady case, the SP_2 equations, which are of order $\mathcal{O}(\varepsilon^4)$, have proven to be inadequate in practice. This is due to their origin from the P_2 equations [7]. Therefore we omit them and proceed with the SP_3 equations.

Noting that Eq. (2.13) has the form of the balance equation (2.5), we write (2.13) as

$$q - \sigma_a \phi = \sigma_t T \phi - \frac{\sigma_t}{3} X^2 \left\{ \phi + \left[1 + \frac{11}{21} \varepsilon^2 X^2 - 3\alpha \varepsilon^2 T \right] \frac{4}{15} \varepsilon^2 X^2 \phi - \left[1 - \varepsilon^2 T + \frac{4}{5} (1 - \alpha) \varepsilon^2 X^2 \right] \varepsilon^2 T \phi \right\} + \mathcal{O}(\varepsilon^6). \quad (2.15)$$

As before, we have isolated terms that contain time-dependent diffusion operators (first-order time and second-order space derivative). The transformation of the asymptotic expansion into the SP_2 system, i.e. the definition of ξ , is unique up to a multiplicative factor. However, for the expansion up to terms of order $\mathcal{O}(\varepsilon^6)$, it is not clear how the substitutions have to be performed. Thus we have introduced a parameter $\alpha \in [0, 1]$ to split the mixed term TX^2 into two parts. We chose the parameter between zero and one in order to get diffusion equations with the correct signs.

Using Neumann's series, we write (2.15) as:

$$q - \sigma_a \phi = \sigma_t T \phi - \frac{\sigma_t}{3} X^2 \left\{ \phi + \left[1 - \frac{11}{21} \varepsilon^2 X^2 + 3\alpha \varepsilon^2 T \right]^{-1} \frac{4}{15} \varepsilon^2 X^2 \phi - \left[1 + \varepsilon^2 T - \frac{4}{5} (1 - \alpha) \varepsilon^2 X^2 \right]^{-1} \varepsilon^2 T \phi \right\} + \mathcal{O}(\varepsilon^6). \quad (2.16)$$

Now we define

$$\phi_2 = \frac{1}{2} \left[1 - \frac{11}{21} \varepsilon^2 X^2 + 3\alpha \varepsilon^2 T \right]^{-1} \left(\frac{4}{15} \varepsilon^2 X^2 \phi \right), \quad (2.17a)$$

$$\zeta = \left[1 + \varepsilon^2 T - \frac{4}{5} (1 - \alpha) \varepsilon^2 X^2 \right]^{-1} (\varepsilon^2 T \phi), \quad (2.17b)$$

to obtain the system

$$\frac{1}{v} \partial_t \phi = \frac{1}{3\sigma_t} \nabla_x^2 [\phi + 2\phi_2 - \zeta] - \sigma_a \phi + q, \quad (2.18a)$$

$$\frac{1}{v} \partial_t \phi_2 = \frac{1}{3\sigma_t} \nabla_x^2 \left[\frac{2}{15\alpha} \phi + \frac{11}{21\alpha} \phi_2 \right] - \frac{1}{3\alpha} \frac{\sigma_t}{\varepsilon^2} \phi_2, \quad (2.18b)$$

$$\frac{1}{v} \partial_t \zeta = \frac{1}{3\sigma_t} \nabla_x^2 \left[\phi + 2\phi_2 + \left(\frac{12}{5} (1 - \alpha) - 1 \right) \zeta \right] - \sigma_a \phi + q - \frac{\sigma_t}{\varepsilon^2} \zeta. \quad (2.18c)$$

Without time-dependence, the variable ζ is zero. Moreover, for $\alpha = \frac{2}{3}$ the above equations reduce to the steady-state SP_3 approximation. To obtain a system that is not ill-posed, we must take $0 < \alpha < 0.9$ [7].

2.3 Simplification of the SP_3 System

In [7], the SP_3 equations with $\alpha = 2/3$ were derived from the P_3 moment equations. The variable ϕ_2 can be identified with the second-order Legendre moment of the radiative

intensity. The variable ζ , on the other hand, is an auxiliary variable without a straightforward physical interpretation. Furthermore, $\zeta = 0$ in steady-state. To simplify the SP_3 equations, we therefore make a quasi-steady approximation and neglect ζ . We obtain

$$\frac{1}{v}\partial_t\phi = \frac{1}{3\sigma_t}\nabla_x^2[\phi + 2\phi_2] - \sigma_a\phi + q, \quad (2.19a)$$

$$\frac{1}{v}\partial_t\phi_2 = \frac{1}{3\sigma_t}\nabla_x^2\left[\frac{2}{15\alpha}\phi + \frac{11}{21\alpha}\phi_2\right] - \frac{1}{3\alpha}\frac{\sigma_t}{\varepsilon^2}\phi_2. \quad (2.19b)$$

We call these the SSP_3 (simplified-simplified P_3) equations.

We expect that the time-dependent SP_N equations can be generalized to anisotropic scattering in a similar manner as in the steady-state case [17]. In the derivation of the equations, we assumed a homogeneous medium. In steady-state, a variational analysis yielded the SP_N equations for non-homogeneous media as well as interface and boundary conditions [2, 23]. The only difference for space-dependent coefficients is that the spatial derivatives have to be modified like

$$\frac{1}{\sigma_t}\nabla_x^2 \rightarrow \nabla_x\frac{1}{\sigma_t(x)}\nabla_x.$$

For steady-state problems, this modification of the spatial derivatives is asymptotically correct in planar geometry and we expect that it is asymptotically correct for time-dependent planar geometry problems.

3 Boundary Conditions and Initial Values

In this section, we state boundary conditions for the SP_N equations which have been derived using Marshak's method [20]. Let

$$l_1 = -4 \int_{n \cdot \Omega < 0} (n \cdot \Omega)\psi_b d\Omega, \quad l_2 = 16 \int_{n \cdot \Omega < 0} P_3(n \cdot \Omega)\psi_b d\Omega.$$

For the SP_1 equations, we have

$$n \cdot \nabla_x \phi = \frac{\sigma_t}{\varepsilon} \left(\frac{3}{2}l_1 - \frac{3}{2}\phi \right). \quad (3.1)$$

For SP_3 and SSP_3 , we obtain the boundary conditions:

$$n \cdot \nabla_x \phi = \frac{\sigma_t}{\varepsilon} \left(-\frac{25}{12}\phi + \frac{25}{24}\phi_2 + \frac{3}{2}l_1 + \frac{7}{12}l_2 \right) \quad (3.2a)$$

$$n \cdot \nabla_x \phi_2 = \frac{\sigma_t}{\varepsilon} \left(\frac{7}{24}\phi - \frac{35}{24}\phi_2 - \frac{7}{24}l_2 \right) \quad (3.2b)$$

$$\zeta = 0. \quad (3.2c)$$

3.1 Initial Values

Given an initial particle distribution, it is straight-forward to calculate an initial value for ϕ . From the asymptotic analysis, the physical meaning of the auxiliary variables (ξ , ϕ_2 , ζ) is not obvious. Therefore it is not clear what the appropriate initial conditions for these variables are. In many cases, the initial setting is a steady state. In addition, the time-dependent SP_N equations reduce to the steady-state SP_N equations. For the SP_3 equations, we would have to solve (2.17) for ϕ_2 and ζ . Of course, this gives $\zeta = 0$. Alternatively, ϕ_2 could be identified as the second-order Legendre moment and thus be computed from the initial value for ψ .

4 Numerical Method

We have derived the time-dependent SP_N equations in three spatial dimensions. In the following chapter, we will present numerical results in two spatial dimensions. Therefore, here we also describe the numerical method for two dimensions. It can be generalized, however, in a straightforward way.

Mathematically speaking, the above SP_N models are nonlinear parabolic PDEs. This means that after spatial discretization we are faced with a large scale stiff system. From an ODE point of view, an optimal treatment of this stiffness structure is to apply some L -stable implicit time discretization [4, 12]. From the PDE point of view, the avoidance of order reduction (which may occur above order 2) is equally important for the overall efficiency of the time integrator. Both properties are satisfied by the linearly implicit time discretization of Rosenbrock type behind the code ROS3PL [15]. Note that the popular Crank–Nicolson scheme is not L -stable and even not strongly A -stable, which results in an insufficient filtering of spurious modes. Fully implicit schemes require the iterative solution of finite dimensional nonlinear systems of algebraic equations by some Newton-like method. In contrast, linearly implicit methods realize a simplified Newton method in function space and require only the solution of a fixed number of linear systems per time step. According to their one-step nature, they allow for a rapid change of step sizes and an efficient adaptation of the spatial discretization in each time step. Moreover, a simple embedding technique can be used to estimate the error part arising from time discretization.

Linearly implicit time integrators of Rosenbrock type are implemented in the code family KARDOS [6], which is used to solve our SP_N models. KARDOS is characterized by a combination of Rosenbrock solvers in time with multilevel finite elements in space in the setting of an adaptive Rothe approach, i.e., first time discretization and then spatial discretization. In this setting, both time-step control and dynamic mesh refinement on the basis of a posteriori error estimation can be simultaneously realized [1, 16]. A rigorous analysis for nonlinear parabolic systems has been given in [14], where challenging examples from other fields of science and technology are also included.

Next we want to describe the main ingredients of the adaptive Rothe method as needed for the efficient solution of the above described SP_N models. These models can be written as abstract Cauchy problems of the form

$$H\partial_t U = F(U), \quad U(t_0) = U_0, \quad t > 0, \quad (4.1)$$

where H is a constant regular matrix and the diffusion operators and the boundary conditions are incorporated into the nonlinear function $F(U)$. For example, we have $U = (\phi, \xi, \zeta)^T$ for the SP_3 model. To approximate the vector $U(x, t)$ by values $U_n \approx U(\cdot, t_n)$ at a certain time grid

$$0 = t_0 < t_1 < \dots < t_n < \dots < t_{M-1} < t_M = T, \quad (4.2)$$

we apply the 4-stage third-order Rosenbrock method ROS3PL, which has the recursive form

$$\left(\frac{H}{\tau_n \gamma} - J_n \right) U_{ni} = F \left(U_n + \sum_{j=1}^{i-1} a_{ij} U_{nj} \right) - H \sum_{j=1}^{i-1} \frac{c_{ij}}{\tau_n} U_{nj}, \quad i = 1, \dots, 4, \quad (4.3)$$

$$U_{n+1} = U_n + \sum_{i=1}^4 m_i U_{ni}, \quad (4.4)$$

where $\tau_n = t_{n+1} - t_n$ and $J_n = F'(U_n)$. The defining formula coefficients m_i , a_{ij} , c_{ij} , and γ are given in [15]. The method is L-stable and avoids order reduction.

ROS3PL offers a simple way to estimate the local error. An embedded solution \hat{U}_{n+1} of second order can be computed by replacing the original weights m_i by \hat{m}_i in (4.4). In order to take into account the scale of the problem, the local error estimator is defined by the weighted root mean square norm

$$r_{n+1} = \left(\frac{\|U_{n+1} - \hat{U}_{n+1}\|_{L^2(Z)}^2}{ATOL + RTOL \|U_{n+1}\|_{L^2(Z)}^2} \right)^{1/2}. \quad (4.5)$$

The tolerances $ATOL$ and $RTOL$ have to be selected carefully to furnish meaningful input for the error control. The estimator can be used to propose a new time step by

$$\tau_{n+1} = \frac{\tau_n}{\tau_{n-1}} \left(\frac{TOL_t r_n}{r_{n+1} r_{n+1}} \right)^{1/3} \tau_n, \quad (4.6)$$

where TOL_t is a desired tolerance prescribed by the user [11]. If $r_{n+1} > TOL_t$, the step is rejected and redone. Otherwise the step is accepted and we advance in time.

Observe that the above time discretization scheme has been applied to the abstract Cauchy problem (4.1), i.e., to the initial value problem in function space. This means that the

Rosenbrock discretization scheme (4.3) is a sequence of linear elliptic boundary value problems. The spatial approximation of the vectors U_n is now done by multilevel finite elements. This is described next.

The main idea of multilevel techniques consists of replacing the infinite dimensional solution space by a nested sequence of finite dimensional spaces with successively increasing dimension in order to improve the approximation quality. To construct adaptive spatial meshes, we apply the edge-oriented hierarchical error estimator from [5, 14]. Such estimators are well established to control the adaptive multilevel process producing successively finer meshes and, in spatial multi-scale cases, drastically reducing the size of the arising linear algebraic systems with respect to a prescribed tolerance. Let \mathcal{T}_h be an admissible finite element mesh at $t = t_n$ and S_h^1 be the associated finite dimensional space consisting of all continuous piecewise linear functions. Then the standard Galerkin finite element approximation $U_{ni}^h \in S_h^1$ of the intermediate values U_{ni} in (4.3) satisfies the equation

$$(L_n U_{ni}^h, \phi_h) = (R_{ni}, \phi_h) \quad \text{for all } \phi_h \in S_h^1, \quad (4.7)$$

where L_n is the weak representation of the differential operator on the left-hand side in (4.3) and R_{ni} stands for the entire right-hand side in (4.3). Since the operator L_n is independent of i , its calculation is required only once within each time step. The resulting large scale linear systems are solved by the BICGSTAB algorithm [24] with ILU preconditioning.

After computing the approximate intermediate values U_{ni}^h , a posteriori error estimates can be used to give specific assessment of the error distribution. Consider a hierarchical decomposition

$$S_h^2 = S_h^1 \oplus Z_h^2, \quad (4.8)$$

where Z_h^2 is the subspace that corresponds to the span of quadratic bubble functions corresponding to edges. Defining an a posteriori error estimator $E_{n+1}^h \in Z_h^2$ by

$$E_{n+1}^h = E_{n0}^h + \sum_{i=1}^4 m_i E_{ni}^h, \quad (4.9)$$

with E_{n0}^h approximating the projection error of the initial value U_n in Z_h^2 and E_{ni}^h estimating the spatial error of the intermediate value U_{ni}^h , the local spatial error for a finite element $T \in \mathcal{T}_h$ can be estimated by $\eta_T := \|E_{n+1}^h\|_T$. The error estimator E_{n+1}^h is computed by linear systems which can be derived from (4.7). We get for $i = 0$

$$(L_n E_{n0}^h, \phi_h) = (L_n (U_n - U_n^h), \phi_h) \quad \text{for all } \phi_h \in Z_h^2. \quad (4.10)$$

and for $i = 1, \dots, 4$

$$(L_n E_{ni}^h, \phi_h) = (R_{ni}(E_{n1}^h + U_{n1}^h, \dots, E_{n,i-1}^h + U_{n,i-1}^h), \phi_h) - (L_n U_{ni}^h, \phi_h) \quad \text{for all } \phi_h \in Z_h^2. \quad (4.11)$$

Solving these equations encounters a sequence of five large linear problems in the space of hierarchical surpluses. From many practical computations, we have experienced that using the approximate error estimator

$$E_{n+1}^h \approx \tilde{E}_{n+1}^h = E_{n0}^h + \frac{E_{n1}^h}{\gamma}, \quad (4.12)$$

that is an error estimator for the embedded, locally second order linearly implicit Euler solution $U_{n+1}^{h,euler} = U_n^h + U_{n1}^h/\gamma$, is quite efficient. Combining (4.10) and the first equation of (4.11) yields the following simplified error equation

$$(L_n \tilde{E}_{n+1}^h, \phi_h) = (L_n(U_n - U_{n+1}^{h,euler}) + \frac{R_{n1}}{\gamma}, \phi_h) \quad \text{for all } \phi_h \in Z_h^2. \quad (4.13)$$

Although we have reduced the number of error equations considerably, we still face a fully coupled system over the surplus space Z_h^2 in (4.13). Following the approach given in [5], we take further advantage of a localization strategy. The idea is to replace the bilinear form on the left hand side in (4.13) by a spectrally equivalent block-diagonal preconditioner in the surplus space. Then, the error equation can be simultaneously solved for each bubble function, that is, for each edge in the triangulation. Let $\tilde{E}_{n+1}^{h,loc}$ be the corresponding error estimator. The local spatial error η_T for a finite element $T \in \mathcal{T}_h$ can again be estimated by computing the norm of $\tilde{E}_{n+1}^{h,loc}$ over T . For the overall spatial error, we define in line with the local temporal error in (4.5)

$$||| \tilde{E}_{n+1}^{h,loc} ||| = \left(\frac{\|\tilde{E}_{n+1}^{h,loc}\|_{L^2(Z)}^2}{ATOL + RTOL \|U_{n+1}^h\|_{L^2(Z)}^2} \right)^{1/2}. \quad (4.14)$$

Based on this error estimation, we can control the spatial accuracy of the numerically computed solution to an imposed tolerance level TOL_x . New grid points are placed in regions of insufficient accuracy. Therefore, all elements with $\eta_T > 0.8 \max_T \eta_T$ are refined. We apply the standard red-green refinement technique. The iterative process estimate-refine-solve within a time step is continued until $||| \tilde{E}_{n+1}^{h,loc} ||| < TOL_x$. Obviously, temporal and spatial errors have to be well balanced. We have also to take into account mesh coarsening to gain efficiency. For more details, we refer to [14].

5 Numerical Results

5.1 Marshak Wave

This test case is a two-dimensional version of the analytical Marshak Wave test case from [22]. Here, radiation is coupled to an energy equation for $B \sim T^4$. The heat capacity is chosen such that the problem becomes linear. The equations are

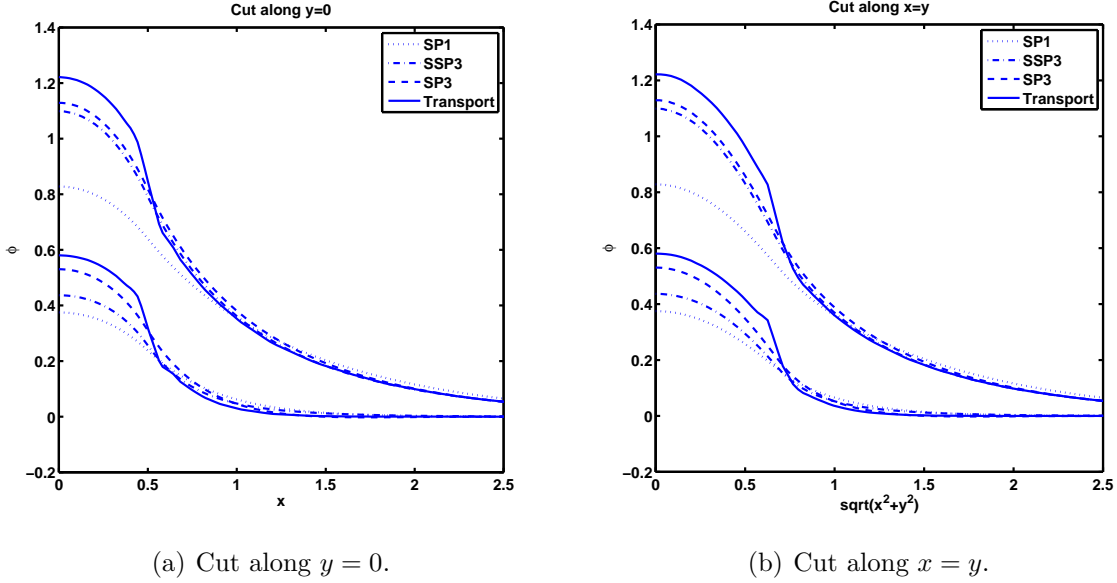


Figure 1: Energy distribution ϕ for different times in 2D Marshak wave.

$$\frac{1}{c} \partial_t \psi(t, x, \Omega) + \Omega \cdot \nabla_x \psi(t, x, \Omega) = \sigma_a(x) (B(t, x) - \psi(t, x, \Omega)) + Q(t, x) \quad (5.1)$$

$$\partial_t B(t, x) = \sigma_a(x) \left(\frac{1}{4\pi} \int_{4\pi} \psi(t, x, \Omega) d\Omega - B(t, x) \right). \quad (5.2)$$

The SP_N approximation is applied to (5.1) and treats the B variable as an additional source term. The additional equation (5.2) is an ordinary differential equation but fits into the numerical framework above.

The setting is two-dimensional and infinite in space ($x \in \mathbb{R}^2$), with time $t \in [0, 10]$. We have $\sigma_a = 1.0$. In an initially empty medium, a spatially bounded source Q is switched on at time zero:

$$Q(t, x) = \begin{cases} \frac{1}{4x_0^2} & \text{for } 0 \leq t \leq t^*, x \in [-x_0, x_0] \times [-x_0, x_0], \\ 0 & \text{otherwise} \end{cases}$$

with $x_0 = 0.5$ and $t^* = 10$.

For symmetry reasons, the computational domain was restricted to $[0, 10] \times [0, 10]$. We set $TOL_t = TOL_x = 10^{-4}$, $RTOL = 1$, $ATOL = 10^{-4}$. The first time step was $\tau_0 = 1.0e - 4$. We started with a criss-cross grid of $20^2 + 21^2 = 841$ points, the largest side length in one triangle being $h = 2^{-1}$. After adaptive refinement, the smallest side length was $h = 2^{-10} \sqrt{2}$. The finest grid consisted of 58916 points (both values extremal for SP_3). Both spatial

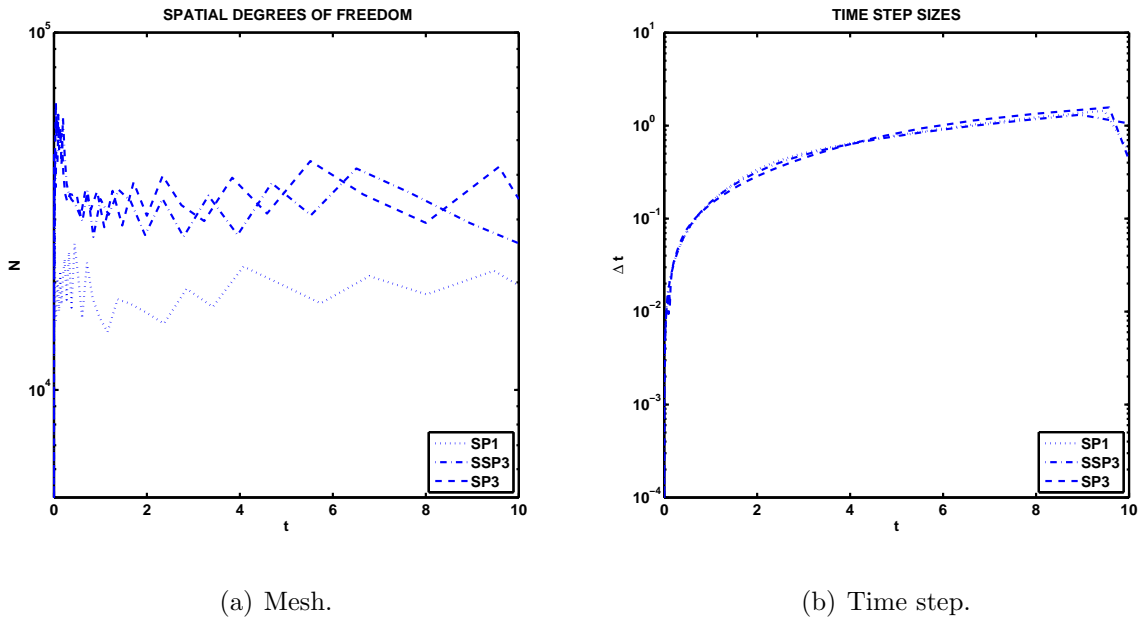


Figure 2: Spatial degrees of freedom (left) and step size (right) as functions of time.

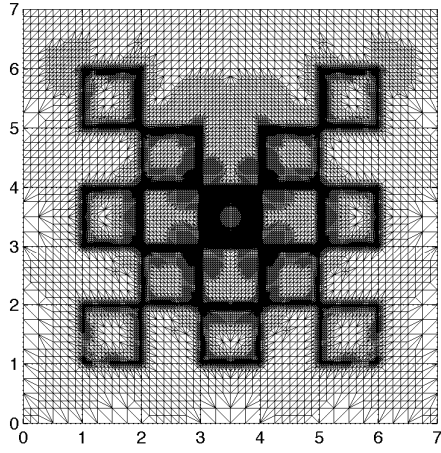
degrees of freedom and the time step are shown in Figure 2. The total computation times were 19m33s (SP_1), 79m10s (SSP_3), 208m53s (SP_3) on a PC with a 3 GHz i686 processor.

In Figure 1, the radiative energy ϕ for times $t = 1$ (lower curves) and $t = 10$ (higher curves) computed by the different models SP_1 , SP_3 , SSP_3 is compared to a benchmark solution (high-order spherical harmonics solution), for both a cut along the x axis as well as a cut along the diagonal $x = y$. As in the one-dimensional case (investigated in [7]), the higher-order diffusion approximations are a clear improvement on the SP_1 diffusion approximation.

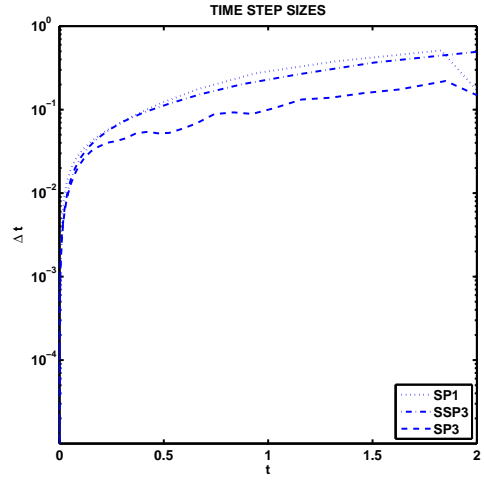
5.2 Lattice Problem

As a more complex numerical test we consider a 2D checkerboard structure of different materials. The geometry, shown in Fig. 3, is identical to the example presented in [3], however modified here to have $\sigma_t = \sigma_s = 0.2 \text{ cm}^{-1}$ in the highly scattering regions (white in Fig. 3), and $\sigma_t = 10 \text{ cm}^{-1}$, $\sigma_s = 0 \text{ cm}^{-1}$ in the highly absorbing regions (grey and hatched squares in Fig. 4(a)). A source (hatched square in Fig. 3) $q = 1$ is switched on at $t = 0$. The final time is $t = 2.0$. The test lies in an intermediate regime between thin and thick media. The radiation field propagates through several obstacles. The main front propagates to the top which is open, but some radiation will leak through the squares.

We set $TOL_t = 10^{-3}$, $TOL_x = 10^{-4}$, $RTOL = 1$, $ATOL = 10^{-7}$ with initial time step

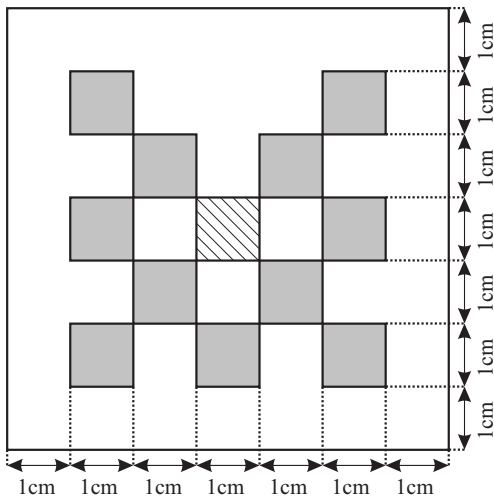


(a) Mesh.

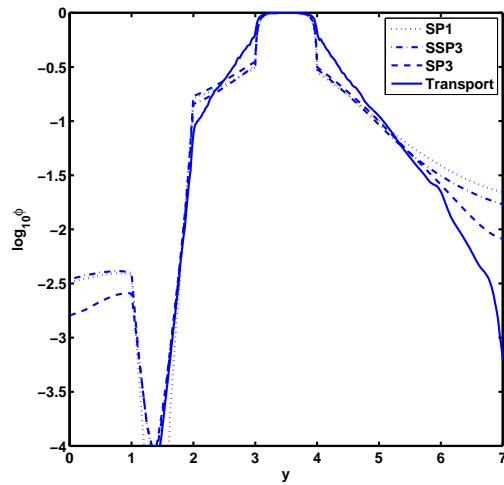


(b) Time step.

Figure 3: Computational mesh for the SP_3 solution at $t = 2.0$ (left) and step size as a function of time (right).

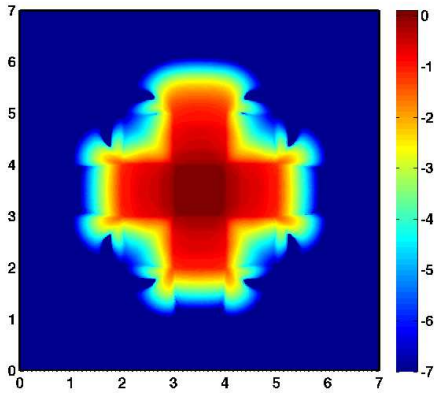


(a) Setting.

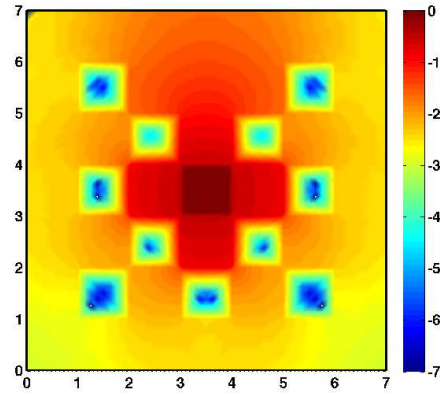


(b) Cut along $x = 3.5$.

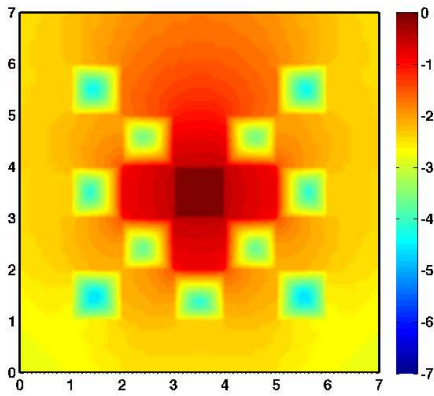
Figure 4: Computational domain for the SP_3 solution (left) and comparison of the different radiative energies along the center line $x = 3.5$.



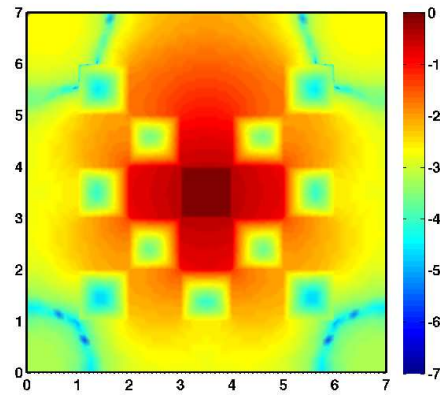
(a) P_7 solution.



(b) SP_1 solution.



(c) SSP_3 solution.



(d) SP_3 solution.

Figure 5: Energy distribution at $t = 2.0$ for different models.

$\tau_0 = 10^{-5}$. Figure 3(a) shows the adaptive grid for the SP_3 solution at $t = 2.0$. It consists of 100100 triangles and 50135 points, the smallest triangle being 2^{-9} . Local refinements can be seen around the jumps at the interfaces between the two media and in the central radiating region. Computation times were 23m46s (SP_1), 58m16s (SPP_3), 164m57s (SP_3) on a PC with a 3 GHz i686 processor.

Figure 5 shows the radiative energy at time $t = 2.0$ on a logarithmic scale. The P_7 solution, which serves as a benchmark here, shows sharp fronts filling the squares adjacent to the center square and a small front escaping on the top. While the radiation in the center region is sufficiently well-described by the diffusion solutions, they overpredict the spreading of the front into the outer regions. However, the SP_3 solution clearly has a smaller and sharper front than the other two lower-order approximations. Quantitatively, this becomes more clear when looking at a cut through the energy profile at $x = 3.5$, shown in Figure 4(b). The escaping front to the top is between $y = 5$ and $y = 7$ and it becomes clear that SP_3 is closest to the benchmark, with SPP_3 having slight advantages over SP_1 .

6 Conclusions

Concerning the validity of the time-dependent SP_N equations, assertions similar to the steady case can be made. Physically, the parabolic scaling and ε small mean that we require the ratio of mean free path and characteristic length scale, as well as the characteristic length divided by the product of characteristic time and velocity to be small of order ε .

The numerical results here and in [7] indicate that the SP_N approximations improve diffusion theory in the sense that not too far away from the diffusive limit a better approximation is obtained.

In the lattice test case, a strong grid refinement around the obstacles was necessary. Similarly, to approximate the effect of source terms well, initially smaller time steps were needed. Using adaptivity in both time and space discretization is essential in many radiative transfer applications. This is especially true for non-homogeneous media with varying coefficients or with source terms.

Acknowledgments

The authors acknowledge support from the German Research Foundation DFG under grant KL 1105/14/2 and SFB 568/3.

References

- [1] F. Bornemann, *An adaptive multilevel approach to parabolic equations. iii. 2d error estimation and multilevel preconditioning*, Comput. Sci. Engrg. **4** (1992), 1–45.
- [2] P. S. Brantley and E. W. Larsen, *The simplified P_3 approximation*, Nucl. Sci. Eng. **134** (2000), 1.
- [3] T. A. Brunner and J. P. Holloway, *Two-dimensional time dependent Riemann solvers for neutron transport*, J. Comput. Phys. **210** (2005), 386–399.
- [4] P. Deuffhard and F. Bornemann, *Scientific computing with ordinary differential equations*, Texts in Applied Mathematics, vol. 42, Springer Verlag, 2002.
- [5] P. Deuffhard, P. Leinen, and H. Yserentant, *Concepts of an adaptive hierarchical finite element code*, Comput. Sci. Engrg. **1** (1989), 3–35.
- [6] B. Erdmann, J. Lang, and R. Roitzsch, *Kardos user's guide*, Konrad-Zuse-Zentrum Berlin, 2002.
- [7] M. Frank, A. Klar, E.W. Larsen, and S. Yasuda, *Time-dependent simplified pn approximation to the equations of radiative transfer*, J. Comput. Phys. **226** (2007), 2289–2305.
- [8] E. M. Gelbard, *Applications of spherical harmonics method to reactor problems*, Tech. Report WAPD-BT-20, Bettis Atomic Power Laboratory, 1960.
- [9] ———, *Simplified spherical harmonics equations and their use in shielding problems*, Tech. Report WAPD-T-1182, Bettis Atomic Power Laboratory, 1961.
- [10] ———, *Applications of the simplified spherical harmonics equations in spherical geometry*, Tech. Report WAPD-TM-294, Bettis Atomic Power Laboratory, 1962.
- [11] K. Gustafsson, M. Lundh, and G. Söderlind, *A PI stepsize control for the numerical solution of ordinary differential equations*, BIT **28** (1988), 270–287.
- [12] E. Hairer and G. Wanner, *Solving ordinary differential equations ii, stiff and differential-algebraic equations*, Springer Series in Computational Mathematics, vol. 14, Springer Verlag, 1996.
- [13] A. Klar, J. Lang, and M. Seaïd, *Adaptive solution of SP_N -approximations to radiative heat transfer in glass*, Int. J. Thermal Sci. **44** (2005), 1013–1023.
- [14] J. Lang, *Adaptive multilevel solution of nonlinear parabolic pde systems. theory, algorithm, and applications*, Lecture Notes in Computational Science and Engineering, vol. 16, Springer Verlag, 2000.

- [15] J. Lang and D. Teleaga, *Towards a fully space-time adaptive FEM for magnetoquasistatics*, IEEE Trans. Magn. **44** (2008), 1238–1241.
- [16] J. Lang and A. Walter, *A finite element method adaptive in space and time for nonlinear reaction–diffusion systems*, Comput. Sci. Engrg. **4** (1992), 269–314.
- [17] E. W. Larsen, J. E. Morel, and J. M. McGhee, *Asymptotic derivation of the multigroup P_1 and simplified P_N equations with anisotropic scattering*, Nucl. Sci. Eng. **123** (1996), 328.
- [18] E. W. Larsen, G. Thömmes, and A. Klar, *New frequency–averaged approximations to the equations of radiative heat transfer*, SIAM J. Appl. Math. **64** (2003), 565–582.
- [19] E. W. Larsen, G. Thömmes, A. Klar, M. Seaïd, and T. Götz, *Simplified P_n approximations to the equations of radiative heat transfer in glass*, J. Comput. Phys. **183** (2002), 652–675.
- [20] R. E. Marshak, *Note on the spherical harmonic method as applied to the milne problem for a sphere*, Phys. Rev. **71** (1947), 443–446.
- [21] J. E. Morel, J. M. McGhee, and E. W. Larsen, *A three-dimensional time-dependent unstructured tetrahedral-mesh SP_N method*, Nucl. Sci. Eng. **123** (1996), 319–327.
- [22] B. Su and G. L. Olson, *An analytical benchmark for non-equilibrium radiative transfer in an isotropically scattering medium*, nn. Nucl. Energy **24** (1997), 1035–1055.
- [23] D. I. Tomasevic and E. W. Larsen, *The simplified P_2 approximation*, Nucl. Sci. Eng. **122** (1996), 309–325.
- [24] H. A. van der Vorst, *BI-CGSTAB: A fast and smoothly converging variant of BI-CG for the solution of nonsymmetric linear systems*, SIAM J. Sci. Statist. **13** (1992), 631–644.